Title

Influence of multi-wavelength laser irradiation of enamel and dentin surfaces at 0.355, 2.94, and 9.4 μm on surface morphology, permeability, and acid resistance

Journal

Lasers in Surgery and Medicine, 49(10)

ISSN

0196-8092

Authors

Chang, Nai-Yuan N
Jew, Jamison M
Simon, Jacob C
et al.

Publication Date

2017-12-01

DOI

10.1002/lsm.22700

Peer reviewed

HHS Public Access

Author manuscript

Lasers Surg Med. Author manuscript; available in PMC 2018 December 01.

Published in final edited form as:

Lasers Surg Med. 2017 December ; 49(10): 913–927. doi:10.1002/lsm.22700.

Influence of multi-wavelength laser irradiation of enamel and dentin surfaces at 0.355, 2.94, and 9.4 μm on surface morphology, permeability, and acid resistance

Nai-Yuan N. Chang, **Jamison M. Jew**, **Jacob C. Simon**, **Kenneth H. Chen**, **Robert C. Lee, DDS, PhD**, **William A. Fried**, **Jinny Cho**, **Cynthia L. Darling, PhD**, and **Daniel Fried, PhD**[α]

Division of Biomaterials and Bioengineering, Department of Preventive and Restorative Dental Sciences, University of California San Francisco, CA 94143

Abstract

Objective—Ultraviolet (UV) and infrared (IR) lasers can be used to specifically target protein, water, and mineral, respectively, in dental hard tissues to produce varying changes in surface morphology, permeability, reflectivity and acid resistance. The purpose of this study was to explore the influence of laser irradiation and topical fluoride application on the surface morphology, permeability, reflectivity, and acid resistance of enamel and dentin to shed light on the mechanism of interaction and develop more effective treatments.

Methods—Twelve bovine enamel surfaces and twelve bovine dentin surfaces were irradiated with various combinations of lasers operating at 0.355 (Freq.-tripled Nd:YAG (UV) laser), 2.94 (Er:YAG laser), and 9.4 μm (CO_2 laser), and surfaces were exposed an acidulated phosphate fluoride gel and an acid challenge. Changes in the surface morphology, acid resistance, and permeability were measured using digital microscopy, polarized light microscopy, near-IR reflectance, fluorescence, polarization sensitive-optical coherence tomography (PS-OCT), and surface dehydration rate measurements.

Results—Different laser treatments dramatically influenced the surface morphology and permeability of both enamel and dentin. CO_2 laser irradiation melted tooth surfaces. Er:YAG and UV lasers, while not melting tooth surfaces, showed markedly different surface roughness. Er:YAG irradiation led to significantly rougher enamel and dentin surfaces and led to higher permeability. There were significant differences in acid resistance among the various treatment groups.

Conclusion—Surface dehydration measurements showed significant changes in permeability after laser treatments, application of fluoride and after exposure to demineralization. CO_2 laser irradiation was most effective in inhibiting demineralization on enamel while topical fluoride was most effective for dentin surfaces.

Keywords

CO_2 laser; Er:YAG laser; UV laser; enamel; dentin; caries inhibition; permeability

[α]To whom correspondence should be addressed: Daniel Fried, Ph.D., Division of Biomaterials and Bioengineering, Department of Preventive and Restorative Dental Sciences, 707 Parnassus Avenue, University of California San Francisco, CA 94143-0758, Daniel.fried@ucsf.edu.

INTRODUCTION

The nature of dental decay or caries in the U.S. has changed markedly due to the introduction of fluoride to the drinking water, the use of fluoride dentifrices and rinses, and improved dental hygiene. Despite these advances, dental caries continues to be the leading cause of tooth loss in the U.S. [1–3]. The development of new conservative methods for inhibiting tooth decay are needed. Several studies over the past forty years have demonstrated that lasers can be used to thermally modify the mineral phase, change the surface morphology, and increase the incorporation of fluoride to increase the acid-resistance of dental enamel. Infrared laser radiation from Er:YAG and CO_2 lasers is highly absorbed by water and the minerals of the tooth structure. High-energy laser irradiation has been shown to cause thermal decomposition and crystalline transformation of carbonated hydroxyapatite to a purer-phase hydroxyapatite with increased acid resistance [4–10]. Although alternative mechanisms for caries inhibition by the laser has been proposed, infrared spectroscopy and x-ray crystallography have been used to clearly establish the correlation of carbonate loss from the mineral phase due to thermal decomposition with increased acid resistance. Furthermore, fluoride application both before and after Er:YAG and CO_2 laser irradiation has been shown to further improve the acid resistance of enamel over laser irradiation alone [8,11–14]. Although the mechanism of synergy between fluoride application and laser irradiation has not been firmly established, it is most likely due to the increased retention of fluoride to the laser treated surfaces. UV light at 0.355 μm from a frequency-tripled Nd:YAG laser has been shown to greatly increase the efficacy of fluoride [15]. We hypothesized that the UV laser etches the protein and lipid around the enamel crystals to expose the mineral. This initially increased the enamel permeability and decreased the acid resistance. However, after adding fluoride, the UV laser + topical fluoride treatment was significantly more effective in inhibiting acid dissolution than fluoride alone.

Similar laser treatments that are effective for enamel have not been effective on dentin. IR spectroscopy and microradiography show that CO_2 laser irradiation transforms the dentin into a hypermineralized (harder) enamel-like hydroxyapatite, similar to the laser-irradiated enamel [16,17]. However, dentin contains 50% collagen and the loss of that collagen matrix induces a large volume contraction. The surface layer of enamel-like transformed dentin is permeated by large cracks through which the acid can penetrate, rendering the laser treatments ineffective [18]. Dentin surfaces have been treated in multiple studies using laser pulse durations varying from a microsecond to seconds to modify progressively thicker layers of dentin, but none of the treatments were effective. This was unfortunate, since more effective methods are needed for the treatment of root caries.

The three lasers investigated in this study have distinctly different effects on the surface morphology of enamel. The CO_2 laser operating at 9.3–9.6 μm, coincident with the strongest absorption by the mineral phase, produces a glass-like layer of melted enamel with an order of magnitude increase in the size of the enamel crystals, and this layer is highly effective in inhibiting acid dissolution. In contrast, the Er:YAG laser is most strongly absorbed by water. The subsurface expansion of water leads to the ablation of enamel without melting the enamel, and the ablated surface does not have the same characteristic melted layer observed

for the CO_2 laser. Even though it has been shown that the surface temperature is much higher for the CO_2 laser than for erbium lasers at the onset of ablation, Er:YAG lasers have been shown to increase the acid resistance of enamel [19]. However, they are not as effective as the CO_2 laser, and the effect is mostly due to peripheral heat accumulation under undesirable irradiation conditions, such as without water. The UV laser at 0.355 μm appears to selectively etch the protein and lipid around the enamel prisms creating yet another unique surface morphology [15].

The purpose of this study was to explore the influence of laser irradiation and topical fluoride application on the surface morphology, permeability, reflectivity, and acid resistance of enamel and dentin to shed light on the mechanism of interaction and to develop more effective treatments. In addition to irradiating samples with the individual laser systems, we also explored irradiating the samples previously irradiated by the Er:YAG and UV lasers a second time by the CO_2 laser after fluoride application. We hypothesize that prior irradiation by the Er:YAG and UV lasers both preferentially removes protein and lipids including the collagen in dentin, and that this can both enhance the adhesion of topical fluoride and reduce crack formation during the subsequent thermal transformation by the CO_2 laser for more effective caries inhibition.

New tools are now available for assessing laser induced changes to enamel and dentin surfaces. Changes in the surface roughness and permeability are important for acid resistance, fluoride retention and the treatment of hypersensitivity. Methods that monitor light scattering and reflectivity can also be used to measure changes in the surface roughness caused by laser irradiation and the severity of demineralization. In this study, we employed digital microscopy, polarization-sensitive optical coherence tomography (PS-OCT), visible light reflectance, and quantitative light fluorescence. High-resolution digital microscopy is valuable since it allows us to view changes on rough surfaces at 1000× magnification. This approach is advantageous over scanning electron microscopy (SEM), which requires a high vacuum environment that can induce morphological changes in dental enamel, such as the formation of microcracks, making it difficult to differentiate the effects caused by the laser from those caused by the SEM vacuum environment.

The permeability of the laser treated surfaces is also important, since a higher permeability will lead to deeper subsurface demineralization. We have investigated optical methods for monitoring permeability changes, since such measurements can be used to assess the activity of carious lesions [20–22]. When lesions become arrested by mineral deposition in the outer layers of the lesion, the diffusion of fluids into the lesion is inhibited. Previous studies have demonstrated that the optical changes due to the loss of water from porous lesions can be used to assess lesion severity with fluorescence, thermal and NIR imaging [23–25]. Artificial and natural lesions on the occlusal and root surfaces manifest a significant and marked decrease in the rate of dehydration if the lesion has a surface zone indicative of an arrested lesion [20,26]. Permeability changes in dentin is also of importance, since it is correlated to sensitivity to tooth pain and the effectiveness of root canal therapies, specifically in bonding composite root fillings and disinfection [27].

The porosity of the outer layers of active lesions is significantly greater than for arrested lesions. This was determined indirectly by thermal and NIR reflectance dehydration imaging [20]. Hence, the rate of water diffusion out of the lesion reflects the degree of lesion activity. Water in the pores at the surface of the lesion absorbs the incident NIR light and reduces surface scattering, causing reduced lesion contrast. Loss of that water during dehydration causes marked increase in reflectivity and lesion contrast. During lesion dehydration, the vaporization of water from the lesion pores causes a decrease in surface temperature in the lesion area, which can be measured with a thermal imaging camera. Thermal imaging at wavelengths from 8000 to 13000 nm had the highest diagnostic performance on artificial dentinal lesions and natural root caries lesions [26]. NIR reflectance imaging showed better performance than thermal imaging for monitoring the dehydration of enamel lesions, but did not perform well on dentin surfaces due to the higher light scattering of sound dentin. Here, we employ both thermal and NIR reflectance methods to measure the surface dehydration rates of the laser-treated dentin and enamel surfaces, respectively, before and after exposure to demineralization.

In this study, bovine enamel and dentin surfaces were irradiated with various combinations of lasers operating at 0.355, 2.94, and 9.4 μm and surfaces were exposed to topical fluoride and acid challenge simulating tooth decay. Changes in the surface morphology, acid resistance and permeability were measured using digital microscopy, polarized light microscopy (PLM), transverse microradiography (TMR), near-IR (NIR) reflectance, fluorescence (QLF), surface dehydration rate measurements, and polarization sensitive-optical coherence tomography (PS-OCT).

MATERIALS AND METHODS

2.1 Sample Block Preparation

Four sets of samples were used: two sets of enamel blocks and two sets of dentin blocks grouped by the wavelengths of laser irradiation. Enamel and dentin blocks (n=24 each), approximately 10–12 mm in length with a width of 2 mm and a thickness of 2 mm were prepared from extracted bovine incisors acquired from a slaughterhouse. For dentin samples, the bovine enamel was removed from the outer surface towards the dentinoenamel junction (DEJ) to expose the dentin. Both enamel and dentin blocks were ground to a 9 μm finish. Each sample was partitioned into seven fiducial windows by etching small incisions 1.5 mm apart across each of the blocks using a laser. Incisions were etched using a radio-frequency (RF) excited industrial CO_2 laser, a Coherent Diamond J-5V Series (Coherent Inc., Santa Clara, CA), operating at 9.4 μm with a pulse duration of 25 μs and a pulse repetition rate of 200 Hz.

2.2 Laser and Fluoride Treatments

Figure 1 shows the workflow of the study design employed. Three different lasers were used to irradiate the sample windows. The samples were scanned across the respective laser beams using computer-controlled XY motion control systems from Newport (Irvine, CA) including ESP-300 and 301 systems and VP25AA and UTM150 stages. A diode pumped solid state (DPSS) Er:YAG laser (Pantec Engineering AG, Liechtenstein) operating at 2.94

μm with fluence of 7.5 J/cm^2 (for enamel) and 3.75 J/cm^2 (for dentin) with a 100 Hz pulse repetition rate and a sample scanning velocity of 5 mm/s; the Tempest frequency-tripled Nd:YAG laser (New Wave Research, Sunnyvale, CA) operating at 0.355 μm with a fluence of 1.43 J/cm^2 (for both enamel and dentin), a 30 Hz pulse repetition rate, and a sample scanning velocity of 1.25 mm/s; and the J5V CO_2 laser with fluence of 0.88 J/cm^2 (for enamel) and 0.52 J/cm^2 (for dentin) at a 100 Hz pulse repetition rate and a sample scanning velocity of 2 mm/s were used. The 355-nm photons are produced using two nonlinear optical crystals to generate the 3rd harmonic of the Nd:YAG laser operating at 1064-nm. The enamel and dentin blocks were further separated into two subgroups (n = 12 each), the Er:YAG-treated group and UV-treated groups. Some windows were also treated with acidulated phosphate fluoride (APF) (Gelato APF Fluoride Gel, Keystone Industries, Gibbstown, NJ) with 1.23% flouride ion and pH of 3.5 for one minute in combination with serial laser treatments. The seven windows for each sample were subjected to different treatments as follows: 1) fluoride only, 2) UV or Er:YAG laser + fluoride, 3) UV or Er:YAG laser + fluoride + CO_2, 4) CO_2 laser + fluoride, 5) control (no treatment), 6) CO_2 laser only, and 7) UV or Er:YAG laser + CO_2 laser.

2.3 Demineralization Regimen

A thin layer of acid-resistant varnish in the form of nail polish, Revlon 270 (New York, NY), was applied to all sides except the top surfaces of the enamel and dentin blocks before exposure to the demineralization solution. Samples were immersed in 40 mL aliquots of the demineralization solution for three consecutive 24-hour periods for three time points of 24, 48, and 72 hours. The demineralization solution, which was maintained at 37°C and pH 5.0, was composed of 2.0 mmol/L calcium, 2.0 mmol/L phosphate, and 75 mmol/L acetate [28]. This dissolution model is a “surface softened” dissolution model designed to produce subsurface dissolution while maintaining an intact surface, and it simulates highly active early lesions.

2.4 Digital Microscopy

Images of the tooth occlusal surfaces were examined using a digital microscopy/3D surface profilometry system, the VHX-1000 from Keyence (Elmwood, NJ) with the VH-Z25 and VH-Z100R lenses with a magnification from 25 to 1000×. Depth composition (DC) images were acquired by scanning the image plane of the microscope and reconstructing a 2D image with all points at optimum focus.

2.5 Visible and Quantitative Light Fluorescence and Near-IR Reflectance

Visible and quantitative light fluorescence (QLF) images were taken by Dino-lite digital microscopes, Edge AM4815ZTL (extended depth of field) and AM4115TW-GFBW (375-nm excitation with 510-nm longpass filter), respectively (BigC, Torrance, CA). NIR images at 1460 nm were taken using a Xeva-2.35–320 Shortwave infrared (SWIR) camera (Xenics, Leuven, Belgium) and a Model SLS202 extended wavelength tungsten-halogen light source (Thorlabs, Newton, NJ).

2.6 Polarization-Sensitive Optical Coherence Tomography (PS-OCT)

An all-fiber-based optical coherence domain reflectometry (OCDR) system with polarization maintaining (PM) optical fiber, high-speed piezoelectric fiber-stretchers, and two balanced InGaAs receivers that was designed and fabricated by Optiphase, Inc., Van Nuys, CA was used. This two-channel system was integrated with a broadband superluminescent diode (SLD) Denselight (Jessup, MD) and a high-speed XY-scanning system, ESP-300 controller and 850G-HS stages from Newport (Irvine, CA) for *in vitro* optical coherence tomography. This system is based on a polarization-sensitive Michelson white light interferometer. The high power (15 mW) polarized SLD source operated at a center wavelength of 1317 nm with a spectral bandwidth full-width at half-maximum (FWHM) of 84 nm. The sample arm was coupled to an AR-coated fiber-collimator to produce a collimated beam with a 6-mm diameter. The beam was focused onto the sample surface using a 20-mm focal length AR-coated planoconvex lens. This configuration provided lateral resolution of approximately 20-μm and an axial resolution of 10 μm in air with a signal to noise ratio of greater than 40–50 dB. The PS-OCT system is completely controlled using LabVIEW software from National Instruments (Austin, TX). The system is described in greater detail in previous work [29,30]. Acquired scans are compiled into *b-scan* files. Image processing was carried out using Igor Pro, data analysis software from Wavemetrics Inc. (Lake Oswego, OR).

Automated methods for determining the lesion depth (LD) and the integrated reflectivity over the lesion depth (ΔR) have been developed. ΔR is calculated from the cross-polarization image and it is analogous to the integrated mineral loss with depth, or ΔZ, measured with transverse microradiography (TMR), the gold standard for the quantification of the severity of demineralization [31–33]. The average LD and ΔR values were calculated across all treatment windows.

2.7 Near-IR and Thermal Dehydration Measurements

Each sample was placed in a mount connected to a high-speed XY-scanning motion controller system (Newport, Irvine, CA) ESP301 controller with 850G-HS stages. Each sample was immersed in the water bath for 30 seconds while being vigorously shaken to enhance water diffusion. After each sample was removed from the water bath, an image was captured as an initial reference image and pressurized air nozzles were activated to dehydrate the sample. The air pressure was set to 15 psi and the computer controlled air nozzles were positioned 4 cm away from the sample. Each measurement consisted of capturing a sequence of images at 4 frames per second for 30 seconds. For each measurement, the air nozzle and the light source were centered on the region of interest (ROI) that encompasses the entire enamel/dentin sample. The dehydration setup was completely automated using LabVIEW software (National Instruments, Austin, TX).

A Model SU320KTSX InGaAs focal plane array (Sensor-Unlimited, Princeton, NJ) with a spectral sensitivity range from 900 nm to 1750 nm, a resolution of 320 × 256 pixels, and an InfiniMite lens (Infinity, Boulder, CO) was used to acquire all the images during the dehydration process. Light from a 150 W fiber-optic illuminator FOI-1 (E Licht Company, Denver, CO) was directed at the sample at an incident angle of approximately 60° to reduce

specular reflection, and the source to sample distance was fixed at 5 cm. A FEL LP series long-pass filter at 1400 nm (Thorlabs) was used for a wavelength range from 1400–1700 nm. Near-IR reflectance images were processed and automatically analyzed using a dedicated program constructed with LabVIEW software. The intensity difference between the final and initial images, ΔI(t=30), was calculated using $I_{30} - I_0$, where I_{30} is the mean intensity at t = 30 seconds and I_0 is the mean intensity prior to turning on the air nozzle.

An infrared (IR) thermography camera, Model A65 from FLIR Systems (Wilsonville, OR) sensitive from 7.5 – 13 μm with a resolution of 640 × 512 pixels, a thermal sensitivity of 50 mK, and a lens with a 13 mm focal length was used to record temperature changes during the dehydration process. Unlike NIR dehydration measurements where a NIR light source is also needed to illuminate the tooth, thermal imaging does not require an additional light source. The ambient room temperature, flowing air temperature and water bath temperature were approximately 21°C (294.15 K) and were consistent throughout the experiment. The object emissivity was set to 0.92, and the atmospheric temperature was set to 294.15 K [34]. While humidity values were not recorded, every sample was measured under the same conditions, where the relative humidity was set at a default value of 50%. Previous studies have shown the area enclosed by the time-temperature curve, ΔQ, can be used as a quantitative measurement of porosity and can be used to discriminate between sound and demineralized enamel *in vitro* [23,24,26]. Thermal images were processed and analyzed using a dedicated program written in LabVIEW. Calibration was carried out via matching the measurements from the initial reference image to the ambient temperature. ΔQ was calculated and averaged among the samples within each subgroup.

2.8 Polarized Light Microscopy (PLM) and Transverse Microradiography (TMR)

After sample imaging was completed, 200 μm thick serial sections for enamel and 300 μm for dentin were cut using an Isomet 5000 saw (Buehler, IL) for PLM and TMR. PLM was carried out using a Model RZT microscope from Meiji Techno Co., LTD (Saitama, Japan) with an integrated digital camera, a EOS Digital Rebel XT from Canon Inc. (Tokyo, Japan). The sample sections were imbibed in water and examined in the bright-field mode with crossed polarizers and a red I plate with 500 nm retardation. PLM images were acquired at 7.5× and 15× magnifications.

A custom built TMR system was used to measure the volume percent mineral content in the areas of demineralization on the tooth sections [35]. High-resolution microradiographs were taken using Cu Kα radiation from a Philips 3100 X-ray generator and a Photonics Science FDI X-ray digital imager (Microphonics, Allentown, PA). The X-ray digital imager consisted of a 1392 × 1040 pixel interline CCD directly bonded to a coherent micro fiber-optic coupler that transfers the light from an optimized gadolinium oxysulfide scintillator to the CCD sensor. The pixel resolution was 2.15 μm and the images were acquired at 10 frames per second. A high-speed motion control system with Newport UTM150 and 850G stages and an ESP300 controller coupled to a video microscopy and a laser targeting system were used for precise positioning of the sample in the field of view of the imaging system.

Average LD values from PLM and ΔZ values from TMR across all treatment windows were compared to the average LD and ΔR values from PS-OCT.

2.9 Statistical Analysis

Groups of dentin and enamel samples were compared using one-way analysis of variance with repeated measures (RM-ANOVA) with Tukey's multiple comparisons post-test using Prism 7 statistical software (GraphPad Software, Inc., La Jolla, CA) for dehydration, PS-OCT, and histological measurements. Significance level was set at $p < 0.05$.

RESULTS

3.1 Surface Morphology

High-resolution digital light microscope images of the laser irradiated enamel and dentin surfaces are shown in Figs. 2 and 3. These are depth convolution images with all the surfaces in focus. The surface morphology varies markedly with the different laser systems. The enamel surfaces irradiated only by the UV and Er:YAG lasers appear rough and melting is not apparent. For the enamel windows irradiated by the CO_2 laser, there are lamellar structures produced by recrystallization of the melted enamel. The size of the lamellar structures varies with larger structures for the samples that were also irradiated by the UV and Er:YAG lasers. Similar structures were observed for dentin; however, the tubules are more clearly visible after UV irradiation and the lamellar melt structures after CO_2 laser irradiation are smaller for dentin and not as dramatically altered by UV and Er:YAG irradiation. Melting was only observed after CO_2 laser irradiation.

Figure 4 shows the visible light reflectance, QLF, NIR-reflectance, PS-OCT (b-scan), and PLM images from one of the enamel samples before demineralization and after 72 hours of demineralization. Under visible light reflectance, the Er:YAG irradiation produced the largest increase in surface roughness and reflectivity for the enamel samples. These changes are visible under QLF, and are most obvious for the Er:YAG-treated samples. The most marked differences were observed in NIR reflectance imaging, where windows treated with both Er:YAG and CO_2 lasers showed great contrast compared with control and other windows. After 3 days of demineralization, changes in surface morphology are difficult to distinguish under visible light reflectance and QLF imaging, but can be observed using NIR imaging and PS-OCT for the Er:YAG-treated enamel samples. However, these changes are less obvious in UV-treated enamel samples under NIR reflectance and PS-OCT imaging.

Figure 5 contains similar imaging panels for one of the dentin samples. CO_2 laser irradiation produced dark discolored surfaces due to thermal decomposition (carbonization) of the collagen, which is visible in QLF, but not in the NIR reflectance images. The discoloration is not as visible for the UV and Er:YAG-irradiated samples, which is consistent with the absence of the melting of the mineral phase, but remained for UV-treated samples after 3 days of demineralization. Differences in morphology were not evident in QLF and NIR reflectance images. However, PS-OCT imaging showed marked changes in lesion depth after 3 days of demineralization.

3.2 PS-OCT: Lesion Depth (LD) and Integrated Reflectivity with Lesion Depth (ΔR)

The mean values of the lesion depth (LD) and integrated reflectivity (ΔR) calculated from the PS-OCT images for the enamel samples are shown in Fig. 6. In the Er:YAG-treated

group, windows treated with CO_2 laser + fluoride and windows treated with CO_2 laser only showed significantly lower mean ΔR compared to control, which indicates significant inhibition. Consistent with lower ΔR values, CO_2 laser + fluoride treated windows and CO_2 laser only-treated windows showed significant shallower LD values compared to the control window. In the UV-treated group, there was no significant difference in ΔR among the windows. However, significantly lower LD values were observed in UV + CO_2 laser-treated windows ($p < 0.05$).

The PS-OCT results for dentin samples are shown in Fig. 7. No significant differences were detected amongst the windows for both Er:YAG-treated and UV-treated samples for ΔR and LD.

3.3 Dehydration Measurements

NIR reflectance dehydration measurements for the enamel samples is shown in Fig. 8. Note that Er:YAG-treated enamel windows demonstrated the greatest porosity/permeability regardless of exposure demineralization, while the windows treated with fluoride demonstrated the lowest porosity. NIR reflectance dehydration measurements for dentin samples are not shown here, as no significant changes were detectable; the high light scattering of sound dentin reduces the contrast for NIR reflectance imaging. There was an overall increase in ΔI after 3-days of demineralization for all the windows.

The shape of the dehydration time-intensity curves varied markedly for enamel. The Er:YAG-treated windows exhibited curves with a more sigmoidal-like shape, most visible after 3 days of demineralization. The UV-treated time-intensity curves are also sigmoidal shaped; however, they were less prominent compared to the Er:YAG-treated windows. The CO_2 laser-treated windows, even in combination with UV (but not with Er:YAG), exhibited more logarithmic-shaped curves. These differences in time-intensity curves indicate large changes in surface morphology. From these curves, we calculated the change in NIR reflectance after 30 seconds, ΔI(t=30), which is shown in Table 3. Overall, intensity differences increased after 3 days of demineralization compared to before acid challenge due to the increased lesion porosity.

Thermal dehydration measurements for the dentin samples are shown in Fig. 9. Note that the Er:YAG and CO_2 laser treated windows produced the greatest changes in temperature after dehydration, while the control windows and fluoride-treated (in combination with laser treatment or not) windows yielded the smallest change. Thermal dehydration measurements for enamel samples are not shown here.

The shape of the dentin thermal dehydration time-temperature curves is similar for all the windows with an initial temperature dip followed by progressive increase in temperature. Prior to acid challenge, fluoride only dentin windows and control windows manifested more complex curves. More specifically, fluoride only windows before demineralization showed the sharpest rise in temperature after the initial dip within the first 20 seconds of dehydration. However, after three days of demineralization, all the curves exhibited similar shapes, and all the samples with added fluoride had a lower temperature rise than the control. From these curves, we calculated ΔQ, or the area under the time-temperature curve

from t=0 to t=30 seconds and the mean values are listed in Table 4. Overall, ΔQ increased after 3 days of demineralization.

3.4 Histology: PLM and Microradiography

Measurements for lesion depth (LD) were also assessed using polarized light microscopy. The results for enamel samples, as shown in Figure 10 and Table 1, showed that the average LD values for any CO_2 laser-treated windows in both laser-treated groups are lower compared to the respective control windows (RM-ANOVA, $p<0.05$). For dentin samples, as shown in Figure 11 and Table 2, even though RM-ANOVA showed statistically significant difference in average LD values ($p<0.05$), only CO_2 + fluoride and UV + CO_2 windows in the UV-treated samples showed significantly decreased average LD values compared to the control window. There was no significant difference between the mean LD values assessed with PLM and PS-OCT ($p>0.05$).

Because mineral changes in dentin are difficult to image under polarized light due to the higher light scattering of dentin, TMR measurements for lesion depth and integrated mineral loss were also carried out to image chanegs in mineral density. The results for dentin samples, as shown in Figure 12 and Table 2, showed that the mean integrated mineral loss, or ΔZ, for Er:YAG + F and CO_2 + F treated samples were significantly higher than the control samples ($p<0.05$). No significant differences were detected amongst the windows within the UV-treated groups. Both Er:YAG-treated and UV-treated groups were statistically significant by laser-treatment groups, measured by RM-ANOVA ($p<0.05$).

DISCUSSION

The different laser treatments significantly altered the surface morphology and permeability of both enamel and dentin. Er:YAG and UV lasers, while did not melt the tooth surfaces, greatly increased the surface roughness and permeability. Er:YAG irradiation led to significantly rougher enamel and dentin surfaces and led to higher permeability. Topical fluoride induced changes in the permeability of dentin, but not enamel. CO_2 laser treatments were most effective in inhibiting demineralization.

We hypothesized that Er:YAG laser and UV laser irradiation of enamel and dentin surfaces will expose the mineral structure by removing water and proteins, respectively, to increase fluoride incorporation. We further hypothesized that subsequent CO_2 laser irradiation would melt the surface to incorporate the applied fluoride to increase acid resistance.

In our previous study of the inhibition of demineralization by the UV laser and fluoride, the reduction in the rate of surface dissolution by fluoride alone was only 10% while the reductions were more than 50% for the UV laser + fluoride [15]. A similar reduction was not observed in this study. In the previous study, surface dissolution measurements were used to assess the resistance to acid dissolution and the study was limited to enamel, while in this study actual subsurface lesions were created in both enamel and dentin. The subsurface lesions better emulate natural lesions and are better for predicting the effect of laser and fluoride treatments on the inhibition of clinical lesions.

We had hoped to see significant differences in caries inhibition amongst the multi-laser-treated surfaces; however, we did not. These results also further demonstrate that the inhibition of demineralization is dominated by the thermally induced mineral changes caused by CO_2 laser irradiation and is not due to changes in the organic content which has been hypothesized by others [36,37]. None of the laser conditions reduced the severity of the subsurface lesions on dentin. We had hypothesized that removal of the collagen by Er:YAG and UV irradiation prior to melting by the CO_2 laser would reduce the large cracks due to contraction and increase inhibition, but that was not observed. So far none of our laser treatments have been successful for inhibiting lesions on dentin. There are a few studies that report successful inhibition of demineralization on dentin after CO_2 laser and fluoride treatments, but those studies employed either surface dissolution measurements or surface micro-hardness measurements [38,39]. Since the outer layer of dentin is converted to a harder enamel-like mineral due to loss of collagen, measurements that only sample the outer surface show a positive outcome. However, since there are large cracks in the enamel-like outer layer there is no inhibition of subsurface lesion formation. Therefore, only studies that measure the inhibition of subsurface lesion formation are reliable.

We did observe large and significant changes in the surface dehydration rates for the different treatments. The surface dehydration rates reflect the surface roughness and permeability of the surface. Such measurements are of particular importance for dentin and may be clinically significant for endodontic therapy and hypersensitivity treatments. Other studies have shown that UV laser irradiation of root dentin can decrease its permeability by occluding the dentinal tubules, which may lead to decrease in hypersensitivity [40]. Er:YAG laser irradiation of dentin has also been shown to decrease hypersensitivity, although it was not as effective as the UV laser [40,41]. Another study indicated that Er:YAG laser irradiation increased permeability [27], which is consistent with the results of this study. Along with other studies, our results here demonstrate the usefulness of dehydration measurements for assessing tooth permeability in its potential clinical applications.

We decided to use APF in this study since it was effective in previous laser studies [8,12,14,17,19]. The low pH of APF etches the enamel for better retention of fluoride. This poses a problem for dentin since a much greater volume of tissue is lost and the extensive etching and change in permeability was detected by the dehydration measurements. Other laser and fluoride studies have utilized neutral pH NaF gels or have added fluoride to the dissolution solution [11, 13, 16, 37, 38]. A neutral pH NaF gel would have been a better choice in this study for use on dentin to avoid the extensive etching.

The use of PS-OCT allowed us to monitor the lesion depth and severity of the treated surfaces throughout the demineralization process. However, excessive surface roughening by the Er:YAG laser interfered significantly with our optical measurements. The lesion depth and severity measurements acquired non-destructively with PS-OCT results were confirmed using PLM and TMR.

CONCLUSIONS

Dehydration measurements showed significant changes in permeability after laser treatments, application of fluoride and after exposure to demineralization. The use of PS-OCT allowed us to monitor the lesion depth and severity of the treated surfaces throughout the demineralization process. However, we have also observed that with the Er:YAG laser roughening the sample surfaces significantly. The scattering of light increased several fold interfering with our optical measurements. The lesion depths and lesion severity measurements taken with PS-OCT results were confirmed using PLM and TMR. Significant decreases in lesion depth and mineral loss for enamel and dentin were only observed for enamel surfaces irradiated with CO_2 lasers, and fluoride-treated surfaces for only dentin.

Acknowledgments

This work was supported by NIH/NIDCR grants R01-DE19631 and R01-DE14698.

References

1. Chauncey HH, Glass RL, Alman JE. Dental caries. Principal cause of tooth extraction in a sample of US male adults. Caries Res. 1989; 23(3):200–205. [PubMed: 2661000]
2. Kaste L, Selwitz R, Oldakowski R, Brunelle J, Winn D, Brown L. Coronal caries in the primary and permanent dentition of children and adolescents 1–17 years of age: United States, 1988–1991. J Dent Res. 1996; 75(Spec No):631–641. [PubMed: 8594087]
3. Winn D, Brunelle J, Selwitz R, et al. Coronal and root caries in the dentition of adults in the United States, 1988–1991. J Dent Res. 1996; 75(Spec No):642–651. [PubMed: 8594088]
4. Meurman JH, Hemmerlé J, Voegel JC, Rauhamaa-Mäkinen R, Luomanen M. Transformation of hydroxyapatite to fluorapatite by irradiation with high-energy CO_2 laser. Caries Res. 1997; 31(5): 397–400. [PubMed: 9286525]
5. Fowler BO, Kuroda S. Changes in heated and in laser-irradiated human tooth enamel and their probable effects on solubility. Calcif Tissue Int. 1986; 38(4):197–208. [PubMed: 3011230]
6. Nelson D, Jongebloed W, Featherstone JDB. Laser irradiation of human dental enamel and dentine. N Z Dent J. 1986; 82(369):74–77. [PubMed: 3461347]
7. Featherstone JDB, Barrett-Vespone NA, Fried D, Kantorowitz Z, Seka W. CO2 Laser Inhibition of Artificial Caries-like Lesion Progression in Dental Enamel. J Dent Res. 1998; 77(6):1397–1403. [PubMed: 9649168]
8. Hsu DJ, Darling CL, Lachica MM, Fried D. Nondestructive assessment of the inhibition of enamel demineralization by CO_2 laser treatment using polarization sensitive optical coherence tomography. J Biomed Opt. 2008; 13(5):054027-054027–9. [PubMed: 19021407]
9. Fried D, Featherstone JDB, Visuri SR, Seka WD, Walsh J, Joseph T. Caries inhibition potential of Er:YAG and Er:YSGG laser radiation. Lasers in Dentistry II; Proc SPIE. 1996; 2672:73–78.
10. Apel C, Schäfer C, Gutknecht N. Demineralization of Er:YAG and Er, Cr:YSGG Laser-Prepared Enamel Cavities in vitro. Caries Res. 2003; 37(1):34–37. [PubMed: 12566637]
11. Kwon YH, Lee J-S, Choi Y-H, Lee J-M, Song K-B. Change of enamel after Er:YAG and CO_2 laser irradiation and fluoride treatment. Photomed Laser Surg. 2005; 23(4):389–394. [PubMed: 16144482]
12. Tagomori S, Morioka T. Combined effects of laser and fluoride on acid resistance of human dental Enamel. Caries Res. 1989; 23(4):225–231. [PubMed: 2790854]
13. Fox JL, Yu D, Otsuka M, Higuchi WI, Wong J, Powell G. Combined effects of laser irradiation and chemical inhibitors on the dissolution of dental enamel. Caries Res. 1992; 26(5):333–339. [PubMed: 1468096]
14. Nobre-dos Santos MN, Featherstone JDB, Fried D. Effect of a new carbon dioxide laser and fluoride on sound and demineralized enamel. Lasers in Dentistry VII. 2001; 4249:169–174.

15. Wheeler CR, Fried D, Featherstone JDB, Watanabe LG, Le CQ. Irradiation of dental enamel with Q-switched λ = 355-nm laser pulses: Surface morphology, fluoride adsorption, and adhesion to composite resin. Lasers Surg Med. 2003; 32(4):310–317. [PubMed: 12696100]
16. Gao X-L, Pan J-S, Hsu C-Y. Laser-Fluoride Effect on root demineralization. J Dent Res. 2006; 85(10):919–923. [PubMed: 16998132]
17. Steiner-Oliveira C, Nobre-dos-Santos M, Zero DT, Eckert G, Hara AT. Effect of a pulsed CO2 laser and fluoride on the prevention of enamel and dentine erosion. Arch Oral Biol. 2010; 55(2):127–133. [PubMed: 20031117]
18. Pashley EL, Horner JA, Liu M, Kim S, Pashley DH. Effects of CO_2 laser energy on dentin permeability. J Endod. 1992; 18(6):257–262. [PubMed: 1402582]
19. Cecchini RCM, Zezell DM, de Oliveira E, de Freitas PM, de Eduardo CP. Effect of Er:YAG laser on enamel acid resistance: Morphlogical and atomic spectrometry analysis. Lasers Surg Med. 2005; 37(5):366–372. [PubMed: 16240417]
20. Lee RC, Darling CL, Fried D. Assessment of remineralization via measurement of dehydration rates with thermal and near-IR reflectance imaging. J Dent. 2015; 43(8):1032–1042. [PubMed: 25862275]
21. Lee RC, Staninec M, Le O, Fried D. Infrared Methods for Assessment of the Activity of Natural Enamel Caries Lesions. IEEE J Sel Top Quantum Electron. 2016; 22(3):102–110.
22. Lee RC, Darling CL, Staninec M, Ragadio A, Fried D. Activity assessment of root caries lesions with thermal and near-IR imaging methods. J Biophotonics. Apr.2016 (in press).
23. Kaneko, K., Matsuyama, K., Nakashima, S. Quantification of early carious enamel lesions by using an infrared camera in vitro. Proceedings of the 4th Annual Indiana Conference; Indianapolis, Indiana: Indiana University School of Dentistry; 1999. p. 83-100.
24. Zakian CM, Taylor AM, Ellwood RP, Pretty IA. Occlusal caries detection by using thermal imaging. J Dent. 2010; 38(10):788–795. [PubMed: 20599464]
25. Usenik P, Bürmen M, Fidler A, Pernuš F, Likar B. Near-infrared hyperspectral imaging of water evaporation dynamics for early detection of incipient caries. J Dent. 2014; 42(10):1242–1247. [PubMed: 25150104]
26. Lee RC, Darling CL, Fried D. Assessment of remineralized dentin lesions with thermal and near-infrared reflectance imaging. Lasers in Denistry XXII; Proc SPIE. 2016; 9692:B1–5.
27. Brugnera A, Zanin F, Barbin EL, Spanó JC, Santana R, Pécora JD. Effects of Er:YAG and Nd:YAG laser irradiation on radicular dentine permeability using different irrigating solutions. Lasers Surg Med. 2003; 33(4):256–259. [PubMed: 14571450]
28. Lee RC, Darling CL, Fried D. Assessment of remineralization in simulated enamel lesions via dehydration with near-IR reflectance imaging. Lasers in Dentistry XXI; Proc SPIE. 2016; 9306:H1–6.
29. Bush J, Davis PG, Marcus MA. All-fiber optic coherence domain interferometric techniques. Fiber Optic Sensor Technology II; Proc SPIE. 2001; 4204:71–80.
30. Ngaotheppitak P, Darling CL, Fried D, Bush J, Bell S. PS-OCT of occlusal and interproximal caries lesions viewed from occlusal surfaces. Lasers in Dentistry XXII; Proc SPIE. 2006; 6137:L1–9.
31. Chan KH, Chan AC, Fried WA, Simon JC, Darling CL, Fried D. Use of 2D images of depth and integrated reflectivity to represent the severity of demineralization in cross-polarization optical coherence tomography. J Biophotonics. 2015; 8(1–2):36–45. [PubMed: 24307350]
32. Arends J, Ruben JL, Inaba D. Major topics in quantitative microradiography of enamel and dentin: R parameter, mineral distribution visualization, and hyper-remineralization. Adv Dent Res. 1997; 11(4):403–414. [PubMed: 9470497]
33. Le MH, Darling CL, Fried D. Automated analysis of lesion depth and integrated reflectivity in PS-OCT scans of tooth demineralization. Lasers Surg Med. 2010; 42(1):62–68. [PubMed: 20077486]
34. Lin M, Liu QD, Xu F, Bai BF, Lu TJ. In vitro investigation of heat transfer in human tooth. Fourth International Conference on Experimental Mechanics; Proc SPIE. 2009; 7522:N1–7.
35. Darling CL, Featherstone JDB, Le CQ, Fried D. An automated digital microradiography system for assessing tooth demineralization. Lasers Dent XV; Proc SPIE. 2009; 7162:T1–6.

36. Hsu C-YS, Jordan TH, Dederich DN, Wefel JS. Effects of Low-energy CO_2 Laser Irradiation and the Organic Matrix on Inhibition of Enamel Demineralization. J Dent Res. 2000; 79(9):1725–1730. [PubMed: 11023270]

37. Hsu C-YS, Jordan TH, Dederich DN, Wefel JS. Laser-matrix-fluoride effects on enamel demineralization. J Dent Res. 2001; 80(9):1797–1801. [PubMed: 11926236]

38. Hossain MMI, Hossain M, Kimura Y, Kinoshita J-I, Yamada Y, Matsumoto K. Acquired acid resistance of enamel and dentin by CO_2 laser irradiation with sodium fluoride solution. J Clin Laser Med Surg. 2002; 20(2):77–82. [PubMed: 12017431]

39. Esteves-Oliveira M, Zezell DM, Ana PA, Yekta SS, Lampert F, Eduardo CP. Dentine caries inhibition through CO_2 laser (10. 6 μm) irradiation and fluoride application, in vitro. Arch Oral Biol. 2011; 56(6):533–539. [PubMed: 21176828]

40. Corrêa Aranha AC, Domingues FB, Franco VO, Gutknecht N, De Paula Eduardo C. Effects of Er:YAG and Nd:YAG Lasers on Dentin Permeability in Root Surfaces: A Preliminary in Vitro Study. Photomed Laser Surg. 2005; 23(5):504–508. [PubMed: 16262582]

41. Birang R, Poursamimi J, Gutknecht N, Lampert F, Mir M. Comparative evaluation of the effects of Nd:YAG and Er:YAG laser in dentin hypersensitivity treatment. Lasers Med Sci. 2007; 22(1):21–24. [PubMed: 17115237]

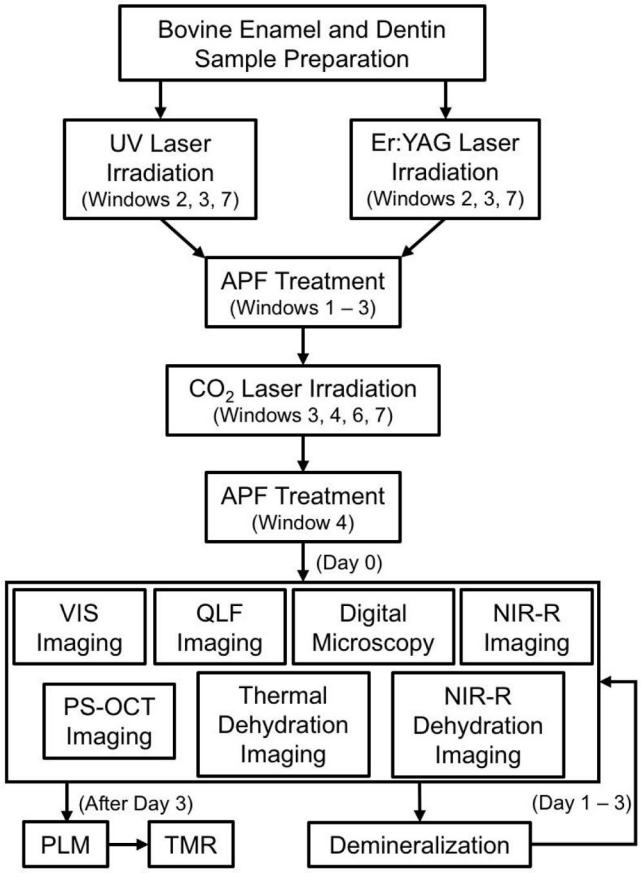

Figure 1.

Workflow of the experimental setup. APF = Acidulated Phosphate Fluoride, VIS = visible light reflectance, QLF = quantitative light fluorescence, NIR-R = near-IR reflectance, PS-OCT = polarization sensitive-optical coherence tomography, PLM = polarized light microscopy, TMR = transverse microradiography.

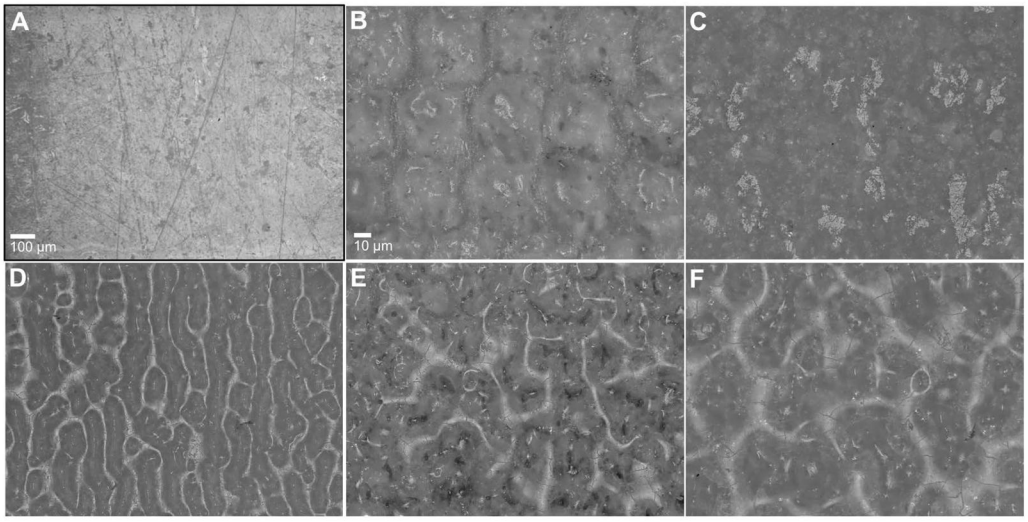

Figure 2.

High-resolution digital light microscope images of enamel surfaces. A) Prior to any treatment (100× magnification; scale-bar = 100 µm); B) Er:YAG treated; C) UV treated; D) CO_2 laser treated; E) Er:YAG and CO_2 laser treated; F) UV and CO_2 laser treated (B – F: 1000× magnification; scale-bar = 10 µm).

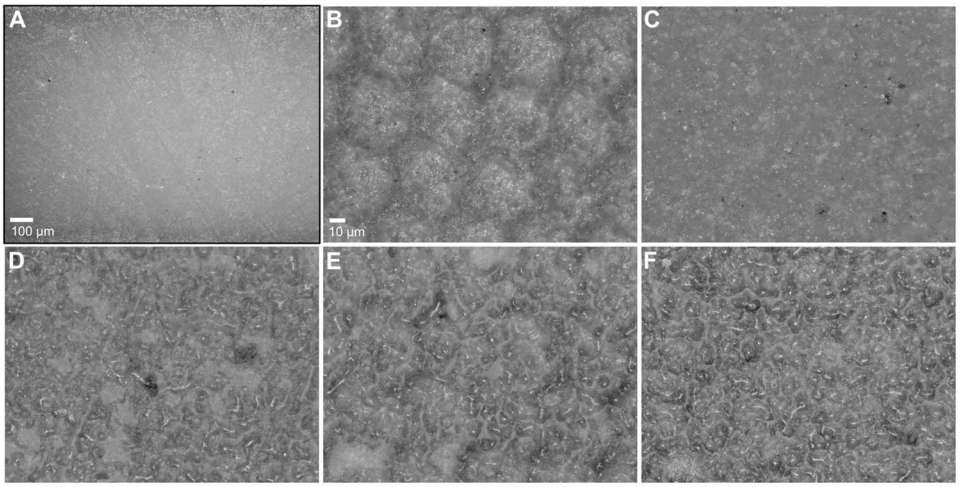

Figure 3.

High-resolution digital light microscope images of dentin surfaces. A) Prior to any treatment (100× magnification; scale-bar = 100 μm); B) Er:YAG treated; C) UV treated; D) CO_2 laser treated; E) Er:YAG and CO_2 laser treated; F) UV and CO_2 laser treated (B – F: 1000× magnification; scale-bar = 10 μm).

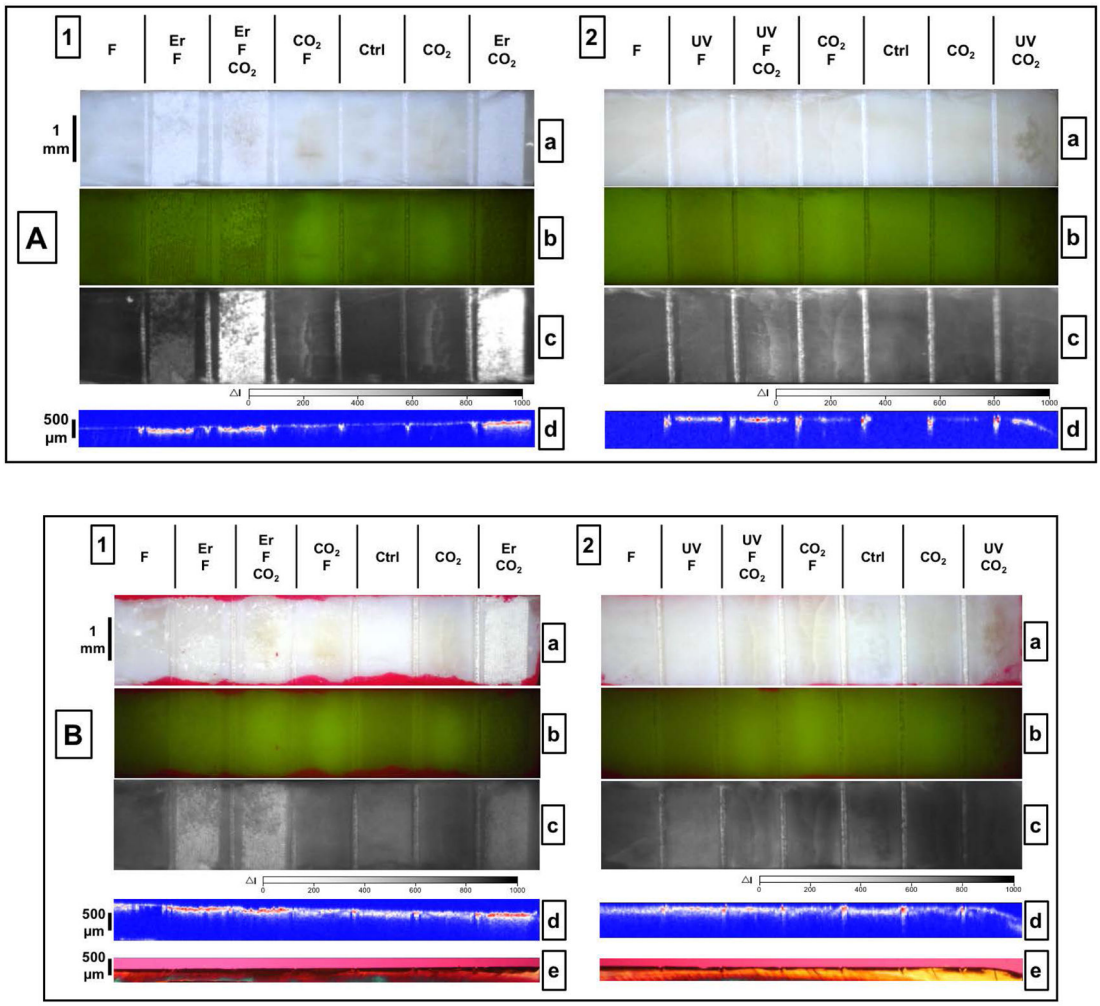

Figure 4.

Images of enamel samples under visible light reflectance, QLF, NIR reflectance, and PS-OCT imaging, and PLM. A) before acid challenge and B) after 3 days of demineralization. 1) Er:YAG-treated sample; 2) UV-treated sample. Inset: a) Visible light reflectance (scale-bar = 1 mm); b) QLF (scale-bar = 1 mm); c) NIR reflectance with a 1460 nm long-pass filter ΔI, intensity differences, from 0 – 1000; scale-bar = 1 mm); d) Processed PS-OCT *s*-B-scan (at 1300 nm; scale-bar = 500 µm); e) PLM (scale-bar = 500 µm).

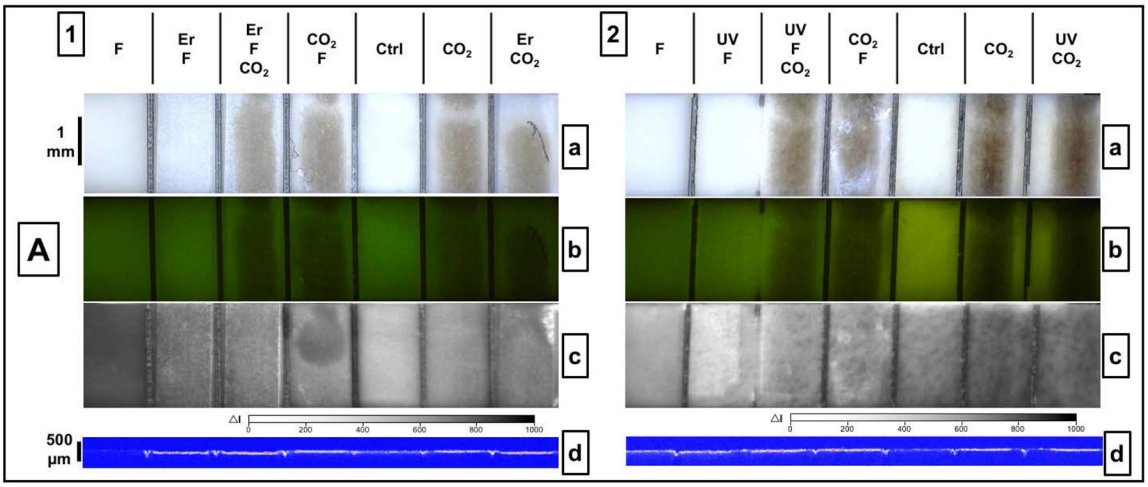

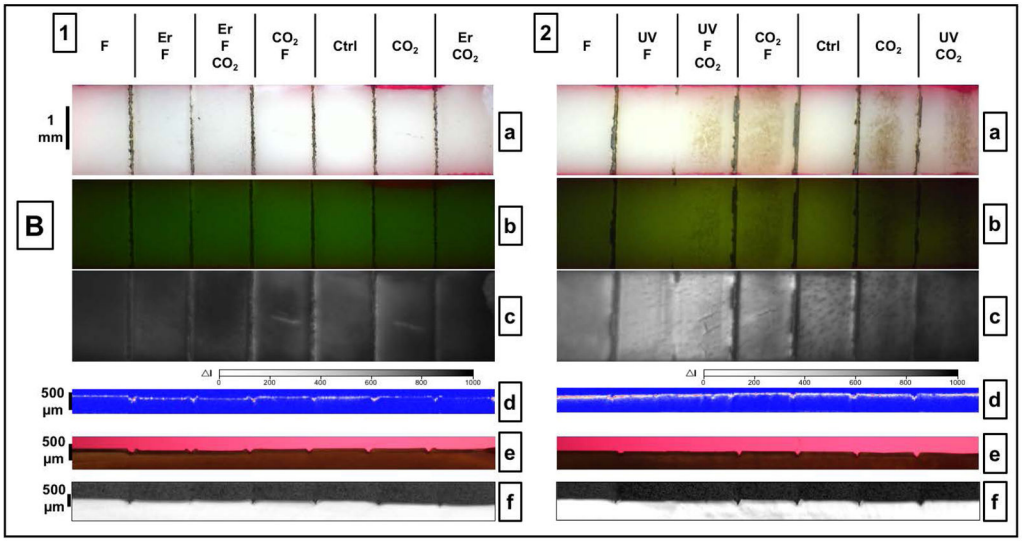

Figure 5.

Images of dentin samples under visible light reflectance, QLF, NIR reflectance, and PS-OCT imaging, and PLM, and TMR A) before acid challenge and B) after 3 days of demineralization. 1) Er:YAG-treated sample; 2) UV treated sample. Inset: a) Visible light reflectance (scale-bar = 1 mm); b) QLF (scale-bar = 1 mm); c) NIR reflectance with a 1460 nm long-pass filter ΔI, intensity differences, from 0 – 1000; scale-bar = 1 mm); d) Processed PS-OCT *s*-B-scan (at 1300 nm; scale-bar = 500 µm); e) PLM (scale-bar = 500 µm); f) TMR.

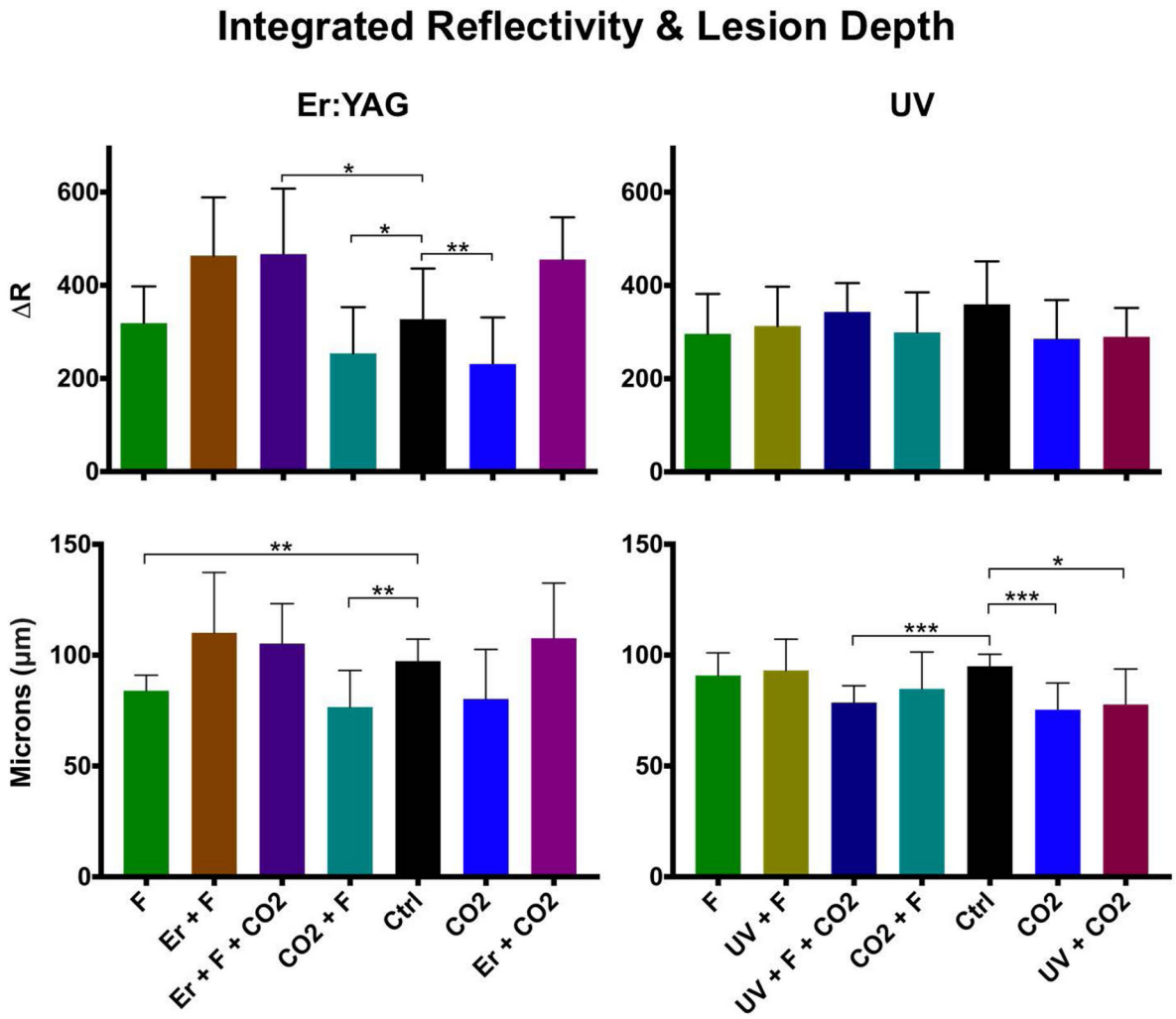

Figure 6.

Integrated Reflectivity, ΔR, and lesion depth (LD in μm) measured for enamel samples after 3 days of demineralization. RM-ANOVA: $p<0.0001$ for both ΔR and LD in Er:YAG-treated group and LD in UV-treated group; $p=0.071$ for ΔR in UV-treated group. Significance level is determined at $p<0.05$; asterisks indicate significant difference compared to Control window.

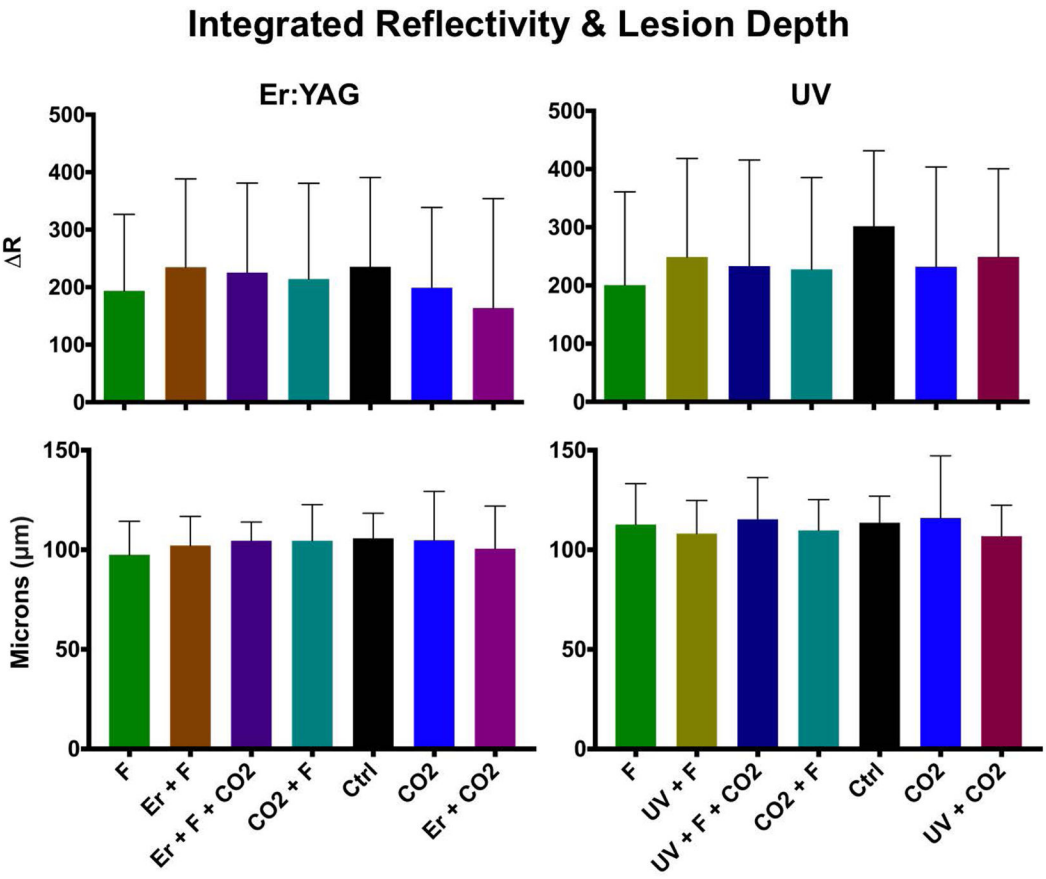

Figure 7.

Integrated Reflectivity, ΔR, and lesion depth (LD in μm) measured for dentin samples after 3 days of demineralization. RM-ANOVA: $p>0.05$ for both treatment groups and both ΔR and LD. Significance level is determined at $p<0.05$; asterisks indicate significant difference compared to Control window.

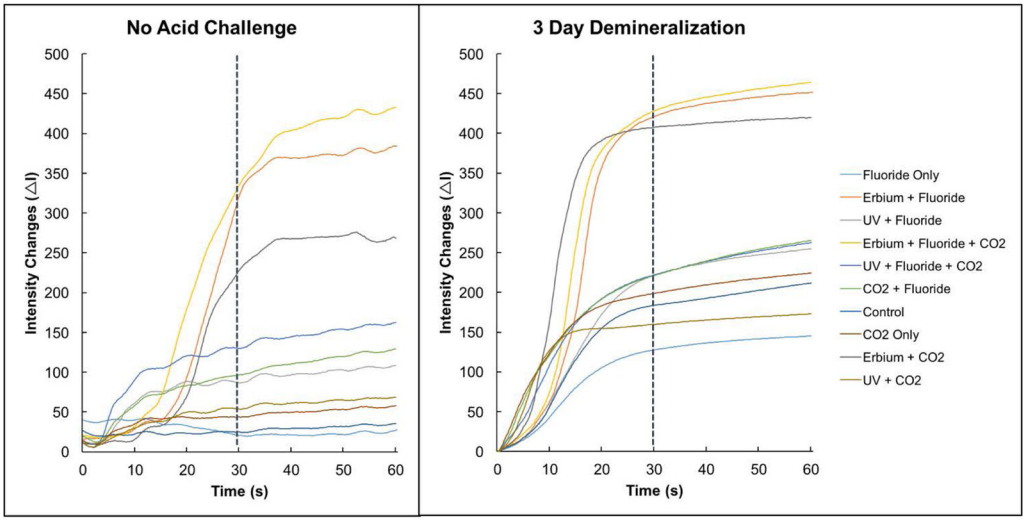

Figure 8.

Average of NIR reflectance dehydration intensity curves for enamel samples (Er:YAG: n = 12, UV: n = 12). Left: no acid challenge; Right: after 3 days of demineralization. The intensity differences between the initial and midpoint NIR reflectance images, ΔI(t=30), for each window were calculated using $I_{30} - I_0$, where I_{30} is the mean intensity at t = 30 seconds and I_0 is the mean intensity prior to turning on the air nozzle. See Table 3 for average ΔI(t=30) values for each window.

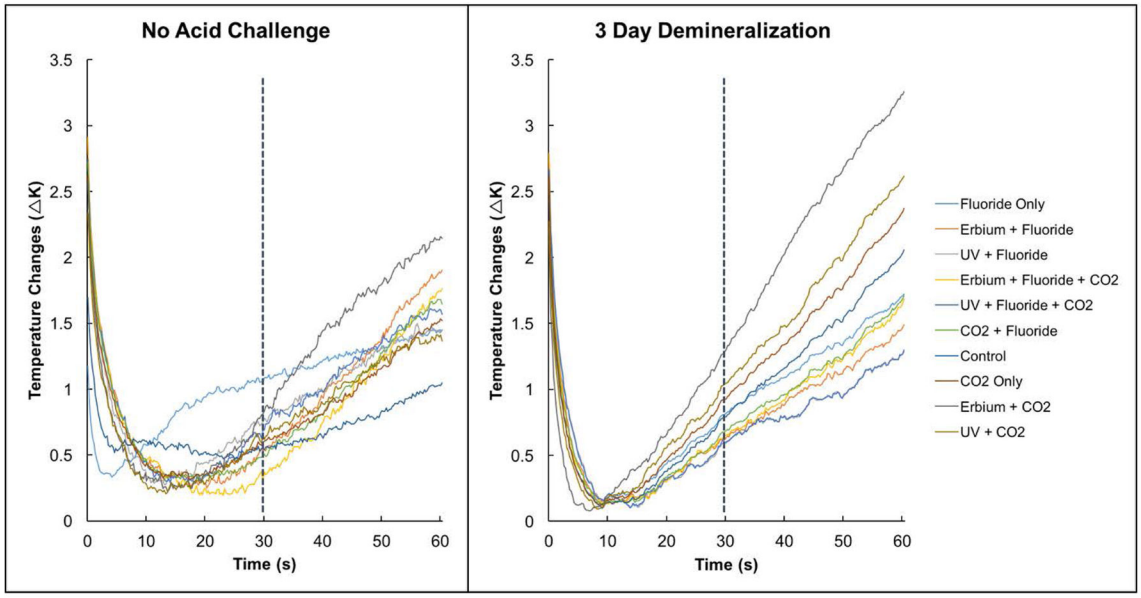

Figure 9.

Average of thermal dehydration time-temperature curves for dentin samples (Er:YAG: n = 12, UV: n = 12). The area enclosed by the time-temperature curve, ΔQ, from initiation of air nozzle to t = 30 seconds were calculated. See Table 3 for average ΔQ values for each window.

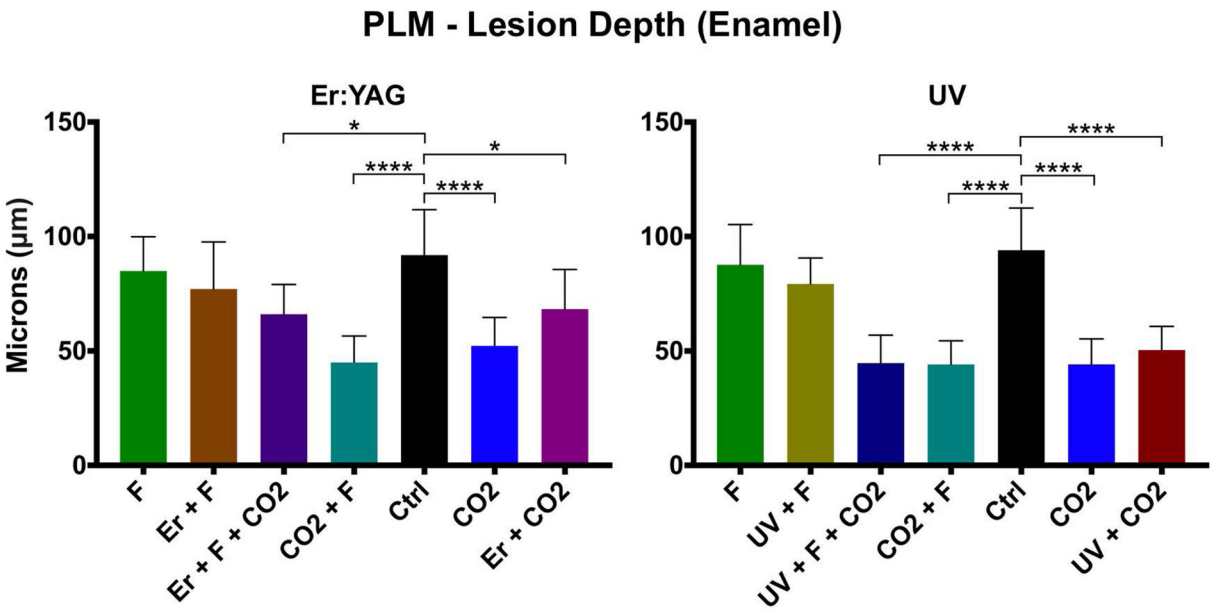

Figure 10.

Average lesion depths of enamel samples measured by PLM (n = 12 for each treatment). Left: Er:YAG-treated samples; right: UV-treated samples. RM-ANOVA: $p<0.0001$ for Er:YAG-treated group; $p<0.0001$ for UV-treated group. Asterisks indicate significant difference compared to Control window.

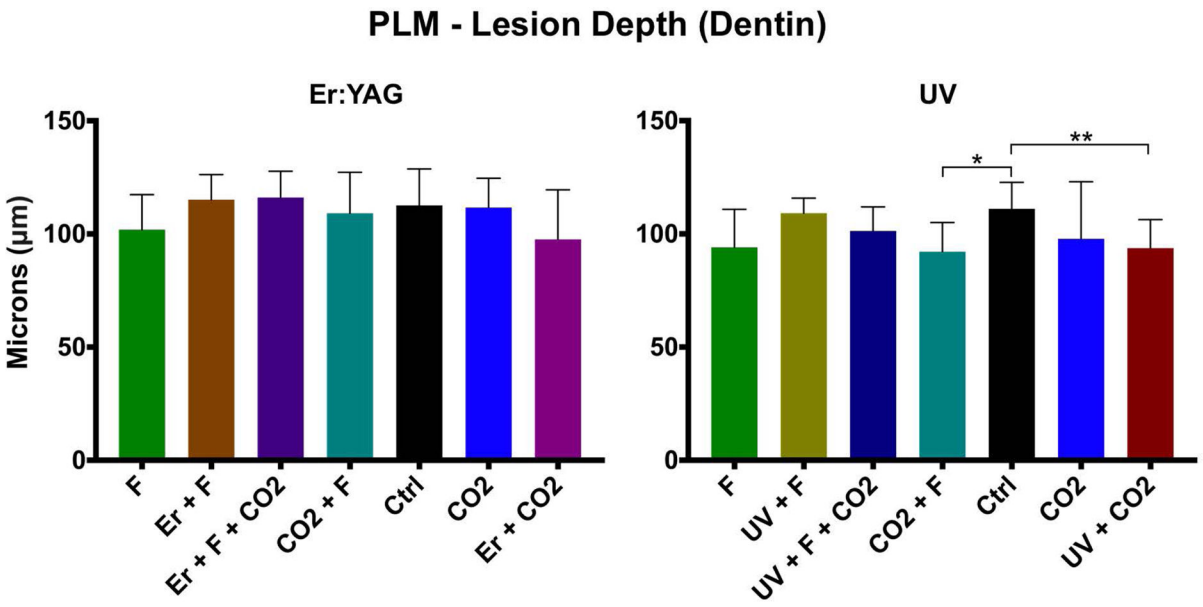

Figure 11.

Average lesion depths of dentine samples measured by PLM (n=12 for each treatment). Left: Er:YAG-treated samples; right: UV-treated samples. RM-ANOVA: p=0.04 for both Er:YAG-treated and UV-treated groups.

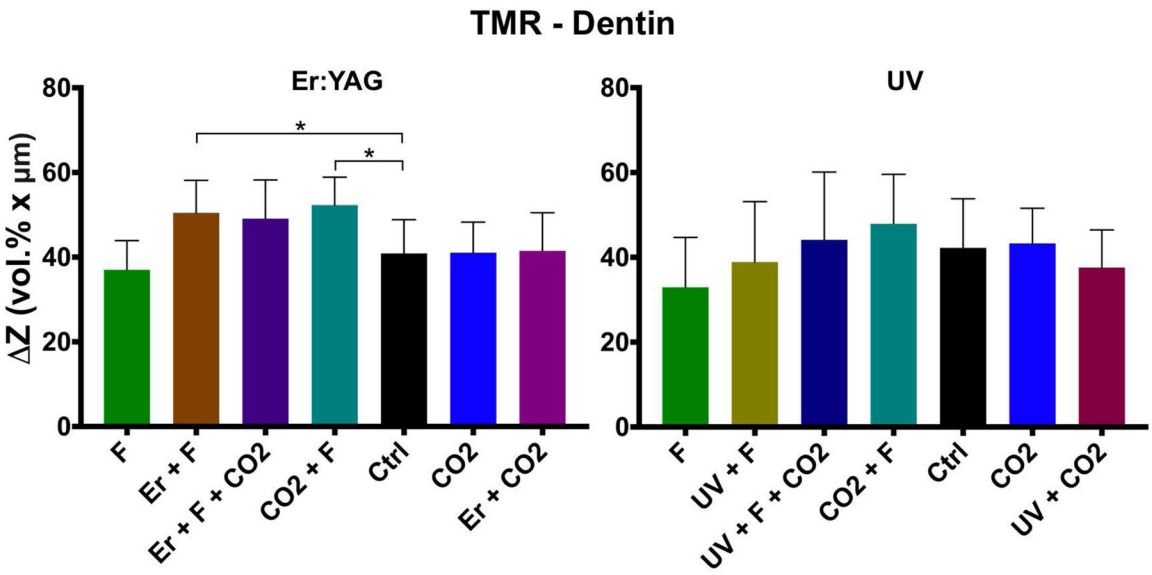

Figure 12.

Average percent integrated mineral loss for dentin samples measured by TMR (n=12 for each treatment). Left: Er:YAG-treated samples; right: UV-treated samples. RM-ANOVA: p=0.0005 for Er:YAG-treated and p=0.033 for UV-treated groups. Asterisks indicate significant difference compared to Control window.

Table 1

PS-OCT and PLM (Enamel)

PS-OCT and PLM results for enamel samples for lesion depth, integrated reflectivity, and integrated mineral loss (mean ± S.D.) for each window after 3 days of demineralization. PS-OCT was imaged using 1300 nm wavelength. Asterisks indicates significant difference compared to the Control window ($p<0.05$).

After 3 Day Demineralization (λ=1300 nm)							
(n = 12)	**F**	**Er:YAG + F**	**Er:YAG + F + CO_2**	**CO_2 + F**	**Ctrl**	**CO_2**	**Er:YAG + CO_2**
Lesion Depth (PS-OCT, μm)	84.0 ± 7.0*	110.1 ± 27.2	105.2 ± 18	76.6 ± 16.6*	97.3 ± 9.9	80.2 ± 22.3	107.6 ± 24.9
Lesion Depth (PLM, μm)	84.9 ± 15.0	77.1 ± 20.5	66.1 ± 13.0*	45.0 ± 11.6*	91.9 ± 19.9	52.2 ± 12.4*	68.3 ± 17.3*
Integrated Reflectivity, ΔR (dB × μm)	319 ± 79	464 ± 125	467 ± 141*	254 ± 99*	327 ± 109	231 ± 100*	455 ± 91
(n = 12)	**F**	**UV + F**	**UV + F + CO_2**	**CO_2 + F**	**Ctrl**	**CO_2**	**UV + CO_2**
Lesion Depth (PS-OCT, μm)	90.8 ± 10.2	93.1 ± 14.1	78.5 ± 7.6*	84.8 ± 16.6	94.9 ± 5.4	75.3 ± 12.1*	77.7 ± 16.0*
Lesion Depth (PLM, μm)	87.7 ± 17.6	79.3 ± 11.3	44.7 ± 12.2*	44.1 ± 10.3*	94.0 ± 18.4	44.1 ± 11.2*	50.5 ± 10.3*
Integrated Reflectivity, ΔR (dB × μm)	296 ± 86	313 ± 84	343 ± 62	299 ± 86	360 ± 92	286 ± 83	290 ± 62

Table 2

PS-OCT, PLM, TMR (Dentin)

PS-OCT, PLM, and TMR results for dentin samples for lesion depth, integrated reflectivity, and integrated mineral loss (mean ± S.D.) for each window after 3 days of demineralization. PS-OCT was imaged using 1300 nm wavelength. Asterisk indicates significant difference compared to the Control window ($p<0.05$).

After 3 Day Demineralization (λ=1300 nm)							
(n = 12)	**F**	**Er:YAG + F**	**Er:YAG + F + CO_2**	**CO_2 + F**	**Ctrl**	**CO_2**	**Er:YAG + CO_2**
Lesion Depth (PS-OCT, μm)	97.5 ± 16.8	102.1 ± 14.6	104.5 ± 9.4	104.5 ± 18.1	105.7 ± 12.7	104.8 ± 24.5	100.5 ± 21.4
Lesion Depth (PLM, μm)	101.9 ± 15.4	115.1 ± 11.1	116.1 ± 11.6	109.1 ± 18.1	112.6 ± 16.1	111.7 ± 13.0	97.5 ± 21.9
Integrated Reflectivity, ΔR (dB × μm)	194 ± 133	235 ± 154	226 ± 156	214 ± 167	235 ± 155	199 ± 140	164 ± 190
Integrated Mineral Loss, ΔZ (vol.% × μm)	37.0 ± 6.9	50.5 ± 7.7*	49.1 ± 9.1	52.3 ± 6.6*	40.9 ± 8.0	41.1 ± 7.2	41.5 ± 9.0
(n = 12)	**F**	**UV + F**	**UV + F + CO_2**	**CO_2 + F**	**Ctrl**	**CO_2**	**UV + CO_2**
Lesion Depth (PS-OCT, μm)	112.7 ± 20.5	108.1 ± 16.7	115.3 ± 20.9	109.7 ± 15.5	113.6 ± 13.3	116.0 ± 31.2	106.8 ± 15.6
Lesion Depth (PLM, μm)	94.1 ± 16.8	109.1 ± 6.6	101.3 ± 10.6	92.2 ± 12.9*	111.0 ± 11.7	97.8 ± 25.2	93.7 ± 12.5*
Integrated Reflectivity, ΔR (dB × μm)	201 ± 160	249 ± 170	233 ± 182	228 ± 158	302 ± 130	232 ± 172	249 ± 152
Integrated Mineral Loss, ΔZ (vol.% × μm)	33.0 ± 11.7	38.9 ± 14.2	44.1 ± 16.0	47.9 ± 11.7	42.2 ± 11.6	43.3 ± 8.3	37.6 ± 8.9

Table 3

ΔI (Enamel)

Enamel NIR dehydration results for each window from before acid challenge to after 3 days of demineralization (mean ± S.D.). NIR dehydration was imaged using 1450 nm wavelength. Asterisks indicates significant difference compared to the Control window ($p<0.05$).

Before Demineralization (λ=1450 nm)							
(n = 12)	**F**	**Er:YAG + F**	**Er:YAG + F + CO_2**	**CO_2 + F**	**Ctrl**	**CO_2**	**Er:YAG + CO_2**
$\Delta I_{(t=30)}$	−16 ± 38	306 ± 287	315 ± 214	70 ± 50	1 ± 26	31 ± 15	217 ± 151
(n = 12)	**F**	**UV + F**	**UV + F + CO_2**	**CO_2 + F**	**Ctrl**	**CO_2**	**UV + CO_2**
$\Delta I_{(t=30)}$	−22 ± 24	74 ± 52	119 ± 55	84 ± 60	−5 ± 32	28 ± 35	43 ± 29
After 3 Day Demineralization (λ=1450 nm)							
(n = 12)	**F**	**Er:YAG + F**	**Er:YAG + F + CO_2**	**CO_2 + F**	**Ctrl**	**CO_2**	**Er:YAG + CO_2**
$\Delta I_{(t=30)}$	131 ± 46	421 ± 170*	428 ± 178*	226 ± 49	192 ± 86	209 ± 40	407 ± 143*
(n = 12)	**F**	**UV + F**	**UV + F + CO_2**	**CO_2 + F**	**Ctrl**	**CO_2**	**UV + CO_2**
$\Delta I_{(t=30)}$	124 ± 55*	222 ± 62	222 ± 59*	216 ± 76*	175 ± 77	188 ± 68	160 ± 56

Table 4

ΔQ (Dentin)

Dentin thermal dehydration results for each window from before acid challenge to after 3 days of demineralization (mean ± S.D.). Thermal dehydration was imaged using 7.5 to 13.5 μm in wavelengths. Asterisks indicates significant difference compared to the Control window ($p<0.05$).

Before Demineralization (λ=8000 nm)							
(n = 12)	**F**	**Er:YAG + F**	**Er:YAG + F + CO_2**	**CO_2 + F**	**Ctrl**	**CO_2**	**Er:YAG + CO_2**
ΔQ (K•sec)	15.9 ± 12.9	60.4 ± 12.3	61.1 ± 12	57.9 ± 13	29.7 ± 13	53.8 ± 14.4	58.2 ± 18.1
(n = 12)	**F**	**UV + F**	**UV + F + CO_2**	**CO_2 + F**	**Ctrl**	**CO_2**	**UV + CO_2**
ΔQ (K•sec)	13.4 ± 8.3	50.8 ± 10.7	55.4 ± 6.1	52.2 ± 10.7	25 ± 5	46.7 ± 6.2	47.9 ± 11.1
After 3 Day Demineralization (λ=8000 nm)							
(n = 12)	**F**	**Er:YAG + F**	**Er:YAG + F + CO_2**	**CO_2 + F**	**Ctrl**	**CO_2**	**Er:YAG + CO_2**
ΔQ (K•sec)	51.7 ± 6.3*	58.9 ± 4.7	60.8 ± 5.9	59 ± 5.8	60.5 ± 7.2	63.3 ± 8.6	56.2 ± 19.6
(n = 12)	**F**	**UV + F**	**UV + F + CO_2**	**CO_2 + F**	**Ctrl**	**CO_2**	**UV + CO_2**
ΔQ (K•sec)	44.4 ± 8.2*	54.2 ± 6.9	55.9 ± 7.2	56 ± 7.6	51.8 ± 10.8	57 ± 9.5*	54.4 ± 11.1